



Wave inhibition by sea ice enables trans-Atlantic ice rafting of debris during Heinrich events

Till J.W. Wagner^{a,b,*}, Rebecca W. Dell^b, Ian Eisenman^b, Ralph F. Keeling^b, Laurie Padman^c, Jeffrey P. Severinghaus^b

^a University of North Carolina Wilmington, United States of America

^b Scripps Institution of Oceanography, University of California San Diego, United States of America

^c Earth and Space Research, Corvallis, OR, United States of America

ARTICLE INFO

Article history:

Received 6 July 2017

Received in revised form 1 May 2018

Accepted 4 May 2018

Available online 21 May 2018

Editor: M. Frank

Keywords:

icebergs

Heinrich events

ice-rafted debris

melt water

modeling

ABSTRACT

The last glacial period was punctuated by episodes of massive iceberg calving from the Laurentide Ice Sheet, called Heinrich events, which are identified by layers of ice-rafted debris (IRD) in ocean sediment cores from the North Atlantic. The thickness of these IRD layers declines more gradually with distance from the iceberg sources than would be expected based on present-day iceberg drift and decay. Here we model icebergs as passive Lagrangian particles driven by ocean currents, winds, and sea surface temperatures. The icebergs are released in a comprehensive climate model simulation of the last glacial maximum (LGM), as well as a simulation of the modern climate. The two simulated climates result in qualitatively similar distributions of iceberg meltwater and hence debris, with the colder temperatures of the LGM having only a relatively small effect on meltwater spread. In both scenarios, meltwater flux falls off rapidly with zonal distance from the source, in contrast with the more uniform spread of IRD in sediment cores. To address this discrepancy, we propose a physical mechanism that could have prolonged the lifetime of icebergs during Heinrich events. The mechanism involves a surface layer of cold and fresh meltwater formed from, and retained around, large densely packed armadas of icebergs. This leads to wintertime sea ice formation even in relatively low latitudes. The sea ice in turn shields the icebergs from wave erosion, which is the main source of iceberg ablation. We find that sea ice could plausibly have formed around the icebergs during four months each winter. Allowing for four months of sea ice in the model results in a simulated IRD distribution which approximately agrees with the distribution of IRD in sediment cores.

© 2018 Elsevier B.V. All rights reserved.

1. Introduction

Layers of sand found in ocean sediment cores throughout much of the North Atlantic indicate several widespread events during the last glacial period. The sand in these layers is too coarse to have been carried by winds or currents, and it is generally believed that this sand was rafted by icebergs during episodes of massive calving from the Laurentide Ice Sheet, called Heinrich events (Heinrich, 1988; Broecker, 1994; Hemming, 2004; Rhodes et al., 2015). These ice-rafted debris (IRD) layers are particularly pronounced in the latitude range 40°N–55°N, which is sometimes referred to as the “IRD belt” (Fig. 1). Large volumes of freshwater rich with debris are expected to have been released from icebergs to produce the observed IRD layers (Dowdeswell et al., 1995; Hemming, 2004;

Levine and Bigg, 2008; Roberts et al., 2014), with estimated ice discharges up to 100 times greater than that from present-day Greenland (Hemming, 2004). Such freshwater fluxes have been found in models to cause the Atlantic Meridional Overturning Circulation (AMOC) to weaken, which leads to reduced poleward heat transport and regional cooling (Broecker et al., 1985; Manabe and Stouffer, 1997; Levine and Bigg, 2008; Otto-Bliesner and Brady, 2010). Hence investigating the distribution of meltwater and IRD during Heinrich events could inform projections of future climate change in scenarios involving substantial discharges of icebergs from the Greenland Ice Sheet.

The thickness of IRD layers provides an indication of iceberg meltwater release and drift tracks during the Heinrich events. Recent studies have investigated this in coarse-resolution climate models, and they found a persistent mismatch between modeling results and IRD thickness in sediment cores (Jongma et al., 2013; Roberts et al., 2014). Specifically, the models tend to simulate a rapid decline of meltwater input from west to east across

* Corresponding author at: University of North Carolina Wilmington, USA.

E-mail address: wagnert@uncw.edu (T.J.W. Wagner).

the North Atlantic which resembles the distribution of modern iceberg sightings (International Ice Patrol, 2009), implying a similar decline in IRD layer thickness (Jongma et al., 2013; Roberts et al., 2014). Ocean sediment cores, by contrast, show a more gradual decrease from west to east (Hemming, 2004). Here we investigate this mismatch with a Lagrangian iceberg drift and decay model forced by output from a comprehensive global climate model (GCM) simulation. In contrast to previous studies, we use a higher resolution ($\sim 1^\circ$) GCM, but the icebergs we simulate are non-interactive, behaving as passive tracers in the climate system.

2. Model setup and simulations

We use a representation of iceberg drift which evolves iceberg velocity, \vec{v}_i , subject to wind and ocean current drag, the pressure gradient force, and the Coriolis force (Wagner et al., 2017a). Compared to previous iceberg models (Bigg et al., 1997; Jongma et al., 2009; Martin and Adcroft, 2010; Marsh et al., 2015), this formulation is somewhat idealized, with the main approximations being that (i) the pressure gradient force is derived from the ocean velocity field by assuming geostrophy, (ii) iceberg speed is taken to be much smaller than surface wind speed, (iii) drag from sea ice and wave radiation are neglected, (iv) water drag is computed from the surface current alone (ignoring vertical shear), and (v) the forces on the iceberg are taken to be balanced (neglecting acceleration). This allows for an analytical solution for iceberg velocity in terms of surface air velocity, \vec{v}_a , and surface water velocity, \vec{v}_w . The solution can be written (Wagner et al., 2017a) as

$$\vec{v}_i = \vec{v}_w + \gamma \left(-\alpha \hat{k} \times \vec{v}_a + \beta \vec{v}_a \right). \quad (1)$$

Here, \hat{k} is the vertical unit vector. The parameter γ is a measure of the relative strength of the air and water drags, and it depends on the densities of ice, water, and air, as well as the air and water drag coefficients. The coefficients α and β depend on wind speed, iceberg size, and the Coriolis parameter. Equation (1) implies that icebergs drift at an angle $\theta = \tan^{-1}(\alpha/\beta)$, relative to the water velocity, with θ depending primarily on wind strength and iceberg size. This solution (1) enables us to efficiently compute large numbers of non-interactive iceberg trajectories from precomputed surface wind and ocean current fields. More details regarding the derivation of equation (1) and the approximations listed above, as well as expressions for α , β , and γ , are given by Wagner et al. (2017a).

We include a representation of iceberg decay that accounts for three main decay processes (Bigg et al., 1997; Martin and Adcroft, 2010; Wagner et al., 2017a): (i) wind-driven wave erosion, M_e , (ii) turbulent basal melt, M_b , and (iii) side wall erosion from buoyant convection, M_v . Iceberg length, L , width, W , and height, H , evolve according to $dL/dt = dW/dt = M_e + M_v$ and $dH/dt = M_b$, with iceberg volume given by $V = LWH$. The individual decay terms are written as follows:

$$\begin{aligned} M_e &= \frac{1}{12} \left(1 + \cos[\pi A_i^3] \right) (T_w - T_0) S(\vec{v}_a, \vec{v}_w), \\ M_v &= b_1 T_w + b_2 T_w^2, \\ M_b &= c |\vec{v}_w - \vec{v}_i|^{0.8} (T_w - T_i) L^{-0.2}, \end{aligned} \quad (2)$$

where A_i is the fractional sea ice concentration, T_w is the sea surface temperature (SST), $T_0 = -2^\circ\text{C}$, S is the sea state, $b_1 = 8.8 \times 10^{-8} \text{ m s}^{-1} \text{ }^\circ\text{C}^{-1}$, $b_2 = 1.5 \times 10^{-8} \text{ m s}^{-1} \text{ }^\circ\text{C}^{-2}$, $c = 6.7 \times 10^{-6} \text{ m}^{0.4} \text{ s}^{-0.2} \text{ }^\circ\text{C}^{-1}$, and T_i is the temperature of the iceberg which is fixed at -4°C . The sea state, S , is computed using a fit to the

Beaufort Scale. Finally, we include iceberg capsizing using the stability criterion of Wagner et al. (2017b), which corrects errors in the original criterion of Bigg et al. (1997). For our primary set of simulations we approximate that there is no sea ice around the icebergs ($A_i = 0$) since the icebergs occur mainly in locations that do not have sea ice in the GCM simulations. We subsequently examine the role of a local seasonal sea ice cover around the icebergs, in which case we approximate that the sea ice moves with the icebergs and does not impact the iceberg drift. This approximation would break down in situations where the drift of icebergs is influenced substantially by the presence of thick pack ice covering large regions (e.g., in modern-day conditions north of Greenland or in the Weddell Sea).

The iceberg model described above requires three input fields which we take from GCM simulations: \vec{v}_w , \vec{v}_a , and SST. We use output from the Community Climate System Model version 4 (CCSM4), a coupled GCM developed by the National Center for Atmospheric Research, which is run at a nominal 1° horizontal resolution (Gent et al., 2011). We force the iceberg model with two previously run CCSM4 simulations: (i) a simulation of the 20th century with historical forcing that spans the period 1850–2005, which is part of the Coupled Model Intercomparison Project phase 5 (CMIP5), henceforth referred to as “20C”, and (ii) a simulation of the last glacial maximum (LGM) with ice sheets, coastlines, greenhouse gases, and solar forcing specified based on paleoclimate estimates (Brady et al., 2013), henceforth referred to as “LGM”.

For each simulation, we consider surface conditions over a 14-yr period. For 20C this period spans the years 1992–2005. For LGM, this period comprises the final 14 yrs of the 1000-yr simulation. The iceberg model is forced with these time-varying climate fields. The analysis of the model output is focused on long-term mean iceberg decay. This is done by computing the iceberg freshwater flux averaged over the 14-yr study period, which removes much of the model’s internal variability. The scale of the additional contributions from longer-term internal climate variability can be assessed by considering the spread over the 6 available CCSM4 historical model realizations. We find this to be relatively small. For example, the spread among model realizations in the 14-yr mean zonal-mean surface wind is 0.2 m s^{-1} , which is much smaller than the latitudinal variation of the zonal-mean surface wind (Wagner and Eisenman, 2017, their Fig. S1).

Mean climate conditions for 20C and LGM are shown in Fig. 1. The continental shelf waters off the Labrador Coast feature the strong southward Labrador Current in the 20C simulation. During the LGM, the continental shelf was mostly above sea level and no significant western boundary current is simulated off the LGM Labrador Coast. The eastward flowing North Atlantic Current is notably stronger east of $\sim 40^\circ\text{W}$ in the LGM simulation. The wind fields show a generally stronger circulation in the LGM case, with particularly strong northwesterlies over the Labrador Coast and elevated wind speeds in the central Atlantic. This is in agreement with previous estimates of enhanced winds during the LGM, a feature that has been attributed to larger atmospheric temperature gradients (McGee et al., 2010). As expected, SSTs are overall colder in the simulated LGM climate. The spatially-averaged cooling in the northern North Atlantic (35°N – 65°N) is 4.8°C . This is somewhat higher than the extra-tropical northern hemisphere average cooling of 3.7°C computed from the full 1000-yr LGM run (Brady et al., 2013). These values compare to an Atlantic-mean SST cooling of 2.8°C obtained using a recent LGM state estimate (Kurahashi-Nakamura et al., 2017).

We consider 10 iceberg size classes with initial dimensions ranging from $100 \times 67 \times 67 \text{ m}$ to $1500 \times 1000 \times 300 \text{ m}$ (see Table S1 and Wagner et al., 2017b). A total of 25×10^3 icebergs are released (2500 for each size class) at a constant rate of 1 iceberg of each size class every 2 days throughout the simulations, and each

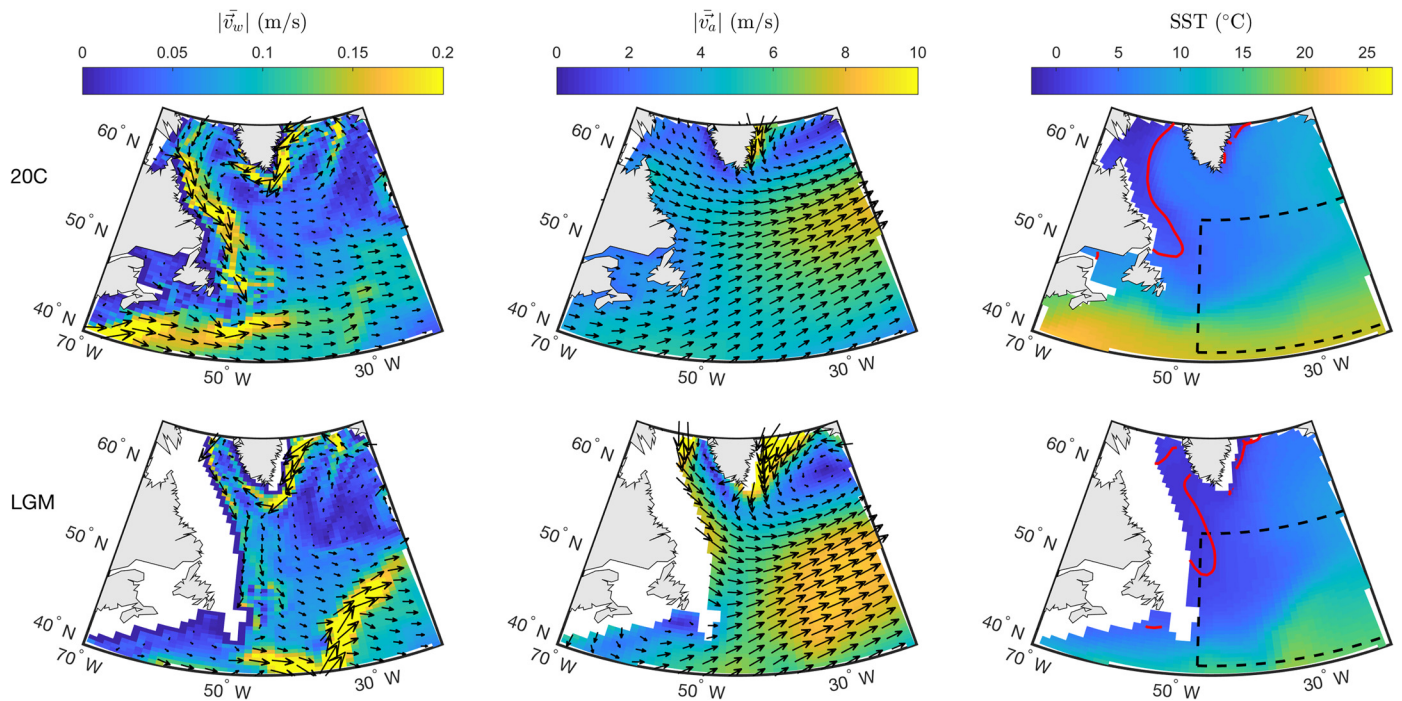


Fig. 1. North Atlantic surface climate conditions in the 20C (top row) and LGM (bottom row) climate model simulations. Left column: surface water velocity (arrows) and speed (shading). The white area indicates the displacement of the coastline at the LGM. Middle column: surface air velocity and speed. Right Column: SST. All fields are averaged over the final 14 yr of the simulations. The red contour lines show the mean March (seasonal maximum) sea ice edge in the study period. The dashed box indicates the area of the IRD belt. (For interpretation of the colors in the figure, the reader is referred to the web version of this article.)

iceberg is tracked until fully decayed. The icebergs move as Lagrangian particles with the precomputed circulation fields. A set of validation runs was previously performed with the 20C fields using seeding locations near three of Greenland's main outlet glaciers (Wagner et al., 2017a), showing reasonably good agreement with the observed range of modern day icebergs as reported by the International Ice Patrol (2009). Note that, like most current GCMs, CCSM4 tends to simulate modern-day surface westerlies that are too strong in the North Atlantic compared to observations. This leads to icebergs being deflected eastward too early, and being confined to latitudes that are slightly too far north (Wagner and Eisenman, 2017).

Release locations are indicated in Fig. 2. The set of iceberg simulations with 20C conditions uses release locations in Baffin Bay, near Hudson Strait and the southern tip of Baffin Island. Because the coastline is displaced at the LGM due to the sea level being reduced by approximately 120 m, LGM icebergs are released approximately 10 degrees further east.

3. Climate conditions, iceberg trajectories, and freshwater input

A subset of the simulated iceberg trajectories are shown in Figs. 2a, b. Note that the iceberg trajectories are computed from the time-varying GCM output fields, rather than the time-averaged fields that are plotted in Fig. 1. The drift patterns between the 20C and LGM sets of iceberg simulations are broadly similar. Note that the different release locations and the resulting proximity of the LGM icebergs to the West Greenland Current complicate direct comparisons between the two sets of simulations. We find that small icebergs are more strongly influenced by the westerly wind forcing (Roberts et al., 2014; Wagner et al., 2017a). Larger icebergs therefore travel farther south in the western boundary current along the Labrador Coast, before they are deflected eastward. LGM icebergs are found to travel somewhat farther south than 20C icebergs, likely aided by the LGM coastline, which extends the western boundary south beyond the modern-day Grand

Banks. The mean longitude of final melt is 33°W in the LGM simulation and 41°W in the 20C simulation (averaged over all size classes, as discussed below). LGM icebergs may be expected to travel considerably further east compared to 20C icebergs for several reasons: LGM icebergs are released 8° further east, westerly wind speeds are overall higher at the LGM, and SSTs are noticeably colder. However, the similarity between the longitudes of final melt appears to be the result of two main factors. (i) Although LGM wind speeds are generally higher, LGM icebergs are released near the somewhat wind-sheltered west coast of Greenland. Wind conditions at the 20C release location tend to be more vigorous. As a result the average wind speeds experienced by 20C and LGM icebergs are almost identical, with $|\vec{v}_a| = 9.1$ and 9.2 m/s, respectively. (ii) 20C icebergs are more rapidly advected by the strong Labrador Current, which is absent at the LGM. The combination of comparable winds and faster ocean currents for 20C icebergs results in slightly higher iceberg drift speeds, with average values of $|\vec{v}_i| = 0.24$ m/s for 20C icebergs and $|\vec{v}_i| = 0.22$ m/s for LGM icebergs. These faster drift speeds compensate almost completely for the longer life span of LGM icebergs, which is 18% longer on average than 20C icebergs due to lower melt rates. As a result, the total distance averaged over all sizes traveled by 20C icebergs (2900 km) is nearly as large as that traveled by LGM icebergs (3000 km).

The average iceberg meltwater distribution is computed from the rate of change in iceberg volume, dV/dt . We define the freshwater input to the ocean as $F(\vec{x}_i, t) \equiv (\rho_i/\rho_w)(dV/dt)$, with ρ_i and ρ_w being the densities of ice and freshwater, respectively, and $\vec{x}_i(t)$ being the position along a given iceberg trajectory. The freshwater flux is F divided by the grid box area. The spatial distributions of time-integrated freshwater flux per 100 km³ of released iceberg volume are shown in Figs. 2d and e for the 20C and LGM simulations, respectively. These are obtained by first computing the freshwater flux for each initial size class. The fluxes are then summed over all classes, weighing each class according to the empirical lognormal distribution of Bigg et al. (1997). This assigns

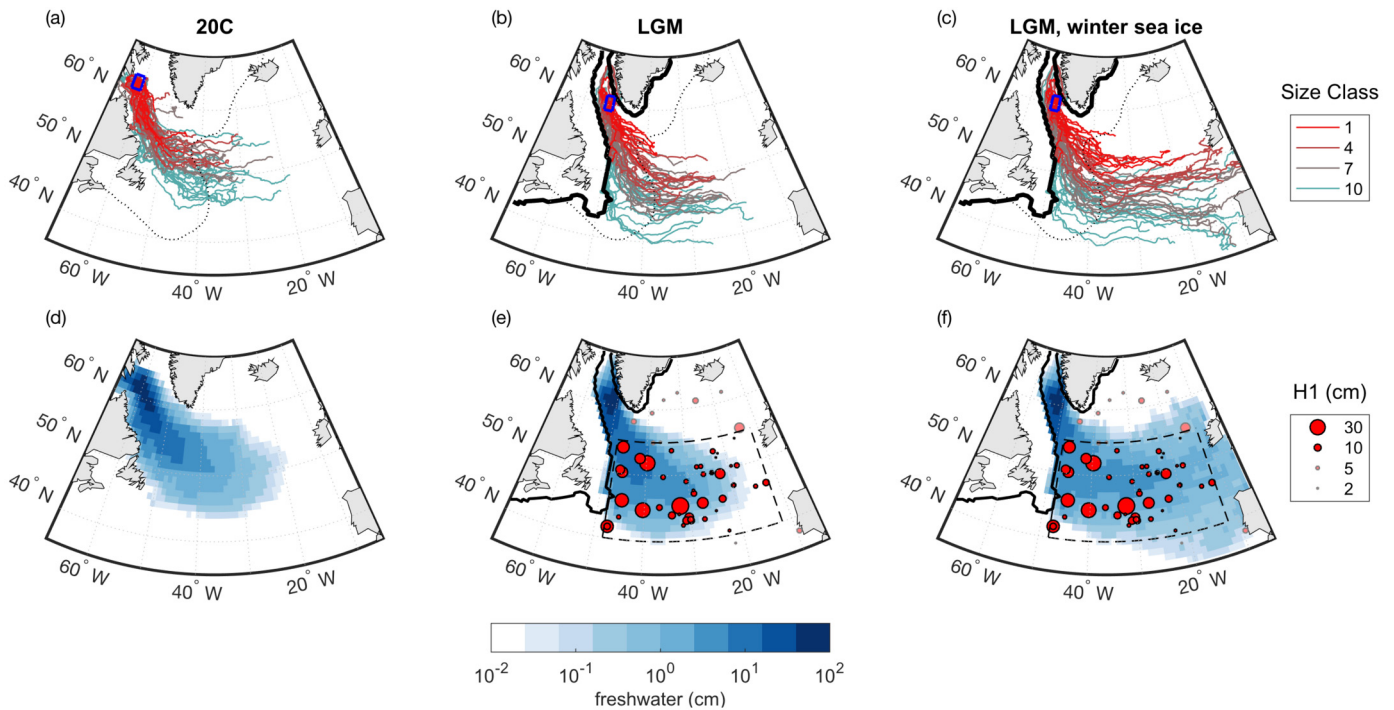


Fig. 2. Modeled iceberg trajectories and freshwater input. (a) 20 trajectories for each of four selected iceberg size classes with 20C climate fields. Colors indicate iceberg size, ranging from smallest in red to largest in green (see legend). Also shown is the typical range of observed modern icebergs (dotted) as reported by the International Ice Patrol (2009). The blue square indicates the region where icebergs are released in the simulations. (b) As in panel a, but for the LGM. The thick black line shows the LGM coastline. (c) As in panel b, but with sea ice added during 4 months of the year to represent a local winter sea ice cover. (d) 20C time-integrated freshwater flux per 100 km³ of iceberg volume released, using a logarithmic color scale. (e) As in panel d, but for the LGM. The red circles indicate the locations of sediment cores considered in this study. Faint red circles indicate cores that are outside the IRD belt. The size of the circles corresponds to the H1 layer thickness, using a logarithmic scale (see legend). The dashed box indicates the IRD belt. (f) As in panel e, but with sea ice added during 4 months of the year.

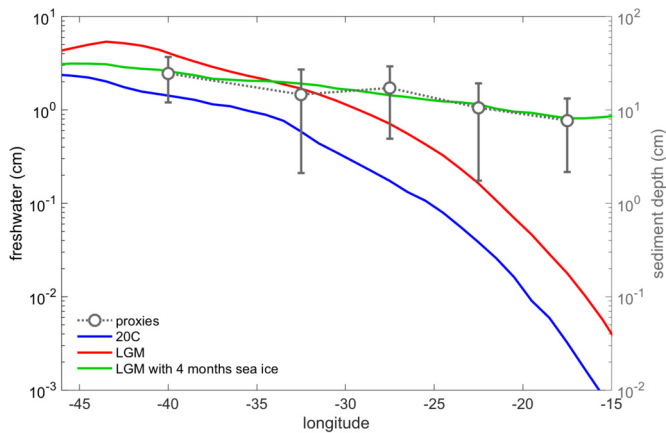


Fig. 3. Dependence of iceberg meltwater and IRD on longitude. The left axis shows mean freshwater released per 100 km³ of iceberg discharge in the LGM (red) and 20C (blue) simulations, averaged over the latitudinal extent of the IRD belt (40°N–55°N). The green curve shows the case where sea ice is added during 4 months of the winter. Here freshwater input is averaged over 1° meridional strips. The right axis indicates the thickness of IRD layers (gray circles) averaged over the events H1, H2, H4, and H5 and over 5 north–south bands within the IRD belt (data from Roberts et al., 2014). The error bars represent the mean plus and minus one standard deviation of the measurements of all four events.

more weight to smaller icebergs which are observed to occur more frequently.

Within the IRD belt, the freshwater distributions for both simulations are found to decrease rapidly with longitude (blue and red curves in Fig. 3). The thickness of the IRD layers in sediment cores (gray error bars in Fig. 3) decreases far more slowly with distance from the Laurentide source than in the simulations. The IRD layer thicknesses shown in Fig. 3 are computed from merid-

ional averages of Heinrich events H1, H2, H4, and H5, as reported by Roberts et al. (2014). Figs. 2e and f illustrate the corresponding core locations and layer thicknesses of Heinrich event 1 for 63 sediment cores within the IRD belt (Dowdeswell et al., 1995; Hemming, 2004). We find that in the model simulations less than 1% of the freshwater reaches beyond 20°W. By contrast, this region features more than 10% of the IRD thickness in sediment cores.

4. Inhibition of wave erosion by sea ice

This discrepancy between the simulations and the sediment core records could be the result of an aspect of the modeled iceberg drift and decay physics being altered during the Heinrich events. Here we consider the processes influencing iceberg decay. In open water, iceberg ablation is primarily caused by wind-driven wave erosion of the iceberg sidewalls (M_e), with the other decay terms (M_v and M_b) typically being substantially smaller (e.g., Marsh et al., 2015). Hence a process that reduces M_e could cause a substantially more extended freshwater distribution (cf. Martin and Adcroft, 2010).

Here we propose a mechanism by which vast armadas of icebergs create their own ocean microclimate that includes an increase in the local sea-ice cover, thereby reducing wave erosion and causing an eastward extension of the distribution of iceberg meltwater.

The decay of icebergs results in a freshwater flux into the upper ocean, which may be expected to initially spread horizontally over a length scale associated with the Rossby radius of deformation in the ocean (10s of km at the latitude of the IRD belt). However, in the presence of large iceberg armadas with a high iceberg density over horizontal length scales much larger than this, the surface freshwater lens may persist. This would cause a shallow halocline, somewhat similar to the modern Arctic Ocean, to form

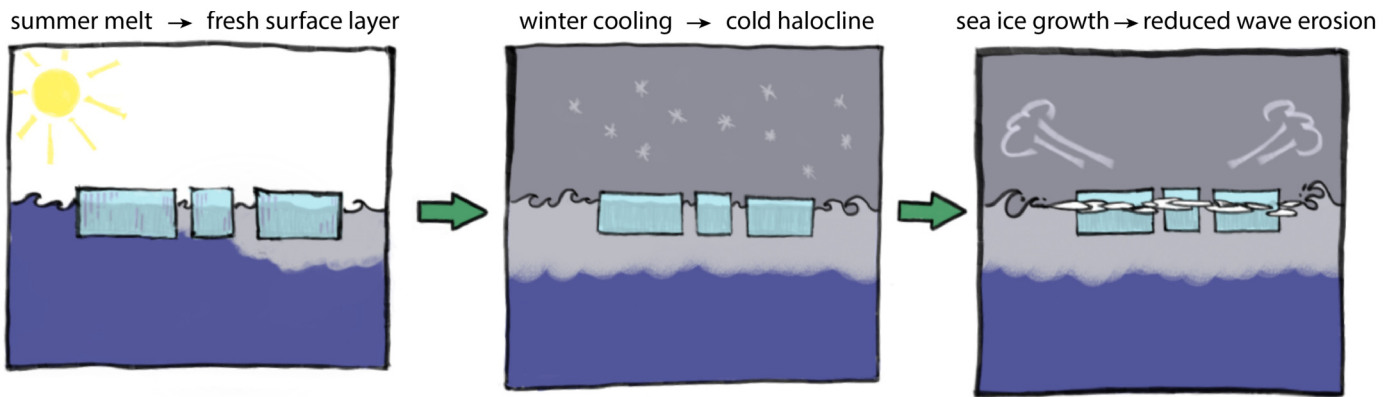


Fig. 4. Proposed mechanism for prolonged iceberg lifetimes. Left: summer melt of icebergs creates a shallow fresh surface layer. Middle: As temperatures drop during fall, the fresh surface layer remains lighter than the saltier waters below. Right: This allows for sea ice to grow as the temperature of the surface layer drops below freezing, which in turn protects the icebergs from wave-induced sidewall erosion and prolongs their lifetimes.

around the iceberg fields. Some indirect evidence that this could occur was gathered serendipitously during previous field work in the Southern Ocean, with observations showing a significant dip in surface salinity and temperature surrounding a small cluster of icebergs that was encountered 500 miles equatorward of the sea ice edge (see Fig S1). In this scenario, as temperatures drop at the end of summer, the surface waters cool without sinking below the shallow halocline created by the meltwater lens. This can allow the surface waters to cool to the freezing point each winter while the saltier waters below remain relatively warm, allowing sea ice to form in relatively low latitudes that would not otherwise have sea ice. This mechanism is summarized in the schematic shown in Fig. 4.

In this scenario, armadas of icebergs in the Atlantic Ocean during Heinrich events would bear some resemblance to the mélanges that form in Greenland's fjords where sea ice sometimes surrounds small clusters of icebergs as they travel through the fjords (e.g., Fig. 1a of Sulak et al., 2017). In the proposed mechanism, substantial concentrations of icebergs over large regions would lead to a similar picture occurring over a far larger scale during winter in the Atlantic Ocean. The clustering of large numbers of icebergs during Heinrich events may have further acted to mechanically confine and protect the sea ice, analogous to the mélanges in present-day fjords.

Note that most state-of-the-art GCMs, including CCSM4, do not include interactive icebergs and hence cannot account for these processes. Furthermore, modeling a realistic halocline in the ocean remains a challenge in current GCMs. In the Arctic Ocean Model Intercomparison Project (AOMIP), ten state-of-the-art Arctic Ocean and sea ice models were analyzed. All ten models failed to accurately reproduce the observed Arctic Ocean halocline, which was attributed in part to inaccurate vertical mixing and shelf-basin exchange processes (see Holloway et al., 2007, their Fig. 1).

A coarser resolution and more idealized Earth System Model of Intermediate Complexity (EMIC) has been used to study Heinrich events with interactive icebergs (Jongma et al., 2013), but the coarse resolution of the EMIC is expected to preclude the simulation of a shallow halocline as pictured in this mechanism.

The representation of wave erosion in Equation (2) includes the sea ice concentration, with wave erosion not occurring ($M_e = 0$) when there is complete sea ice cover ($A_i = 1$). This implies that the sea ice surrounding an armada of icebergs during part of the winter would inhibit wave erosion, nearly eliminating iceberg decay and thereby causing longer iceberg lifetimes and enhanced spatial distribution of meltwater and IRD.

We further assume here that mechanical stirring of the upper ocean due to the iceberg velocity relative to the water is small.

Finally, we do not consider the effect of storm events that may temporarily mix the upper ocean, since a detailed investigation of the strength and reemergence timescale of the halocline in this context is beyond the scope of this study.

We explore the plausibility of the proposed mechanism using back-of-the-envelope calculations involving the CCSM4 LGM simulation output and additional simulations of the Lagrangian iceberg model. The results are summarized here and described in more detail in the SI. Iceberg discharge associated with each Heinrich event is estimated to be approximately $60 \times 10^4 \text{ km}^3$ (Roberts et al., 2014). We assume a typical duration of 500 yrs for a Heinrich event (Hemming, 2004) and consider the case where icebergs meltwater is concentrated within 25% of the area in 40°N – 55°N in the Atlantic Ocean. Using these numbers we find that if approximately 2 months' worth of the freshwater from iceberg discharge became concentrated in the upper 10 m of the ocean column within this region, it would create a halocline that is strong enough to stabilize the water column, even if the temperature of the upper 10 m reached the freezing point in December. That is to say, the water in the upper 10 m could freeze into sea ice rather than sink in a convective plume. Alternatively, in the case where iceberg meltwater is concentrated within 10% of the IRD belt, 2 months' worth of freshwater discharge would stabilize the water column with a 25 m deep surface layer, and in the case where iceberg meltwater is concentrated within 50% of the IRD belt, 2 months' worth of freshwater discharge would stabilize the water column with a 5 m deep surface layer. The sea ice that formed would then insulate the ocean from the atmosphere and thereby substantially reduce the effective surface heat capacity (e.g., Wagner and Eisenman, 2015). We make the somewhat extreme approximation that this stabilization would cause seasonal temperature variations to be as large as they are over land. We find that if the IRD belt had a heat capacity as small as land during the LGM, then it could be expected to be covered by sea ice during 4 months of the year (December through March, Fig. S4). We emphasize, however, that this analysis relies on a number of crude assumptions, and that the final result is dependent on several fairly subjective approximations (see SI for details).

In addition to this freshening, the decaying icebergs further have a cooling effect on the surface layer, due to the latent heat required to melt the ice (cf. Jongma et al., 2013; Bügelmayr et al., 2015). This cooling counteracts the freshening, since cooling increases the density of the surface waters. Here we estimate the magnitude of this effect. We use the linearized state equation for sea water, $\Delta\rho = \rho_0(-\alpha\Delta T + \beta\Delta S)$, where $\rho_0 = 1000 \text{ kg m}^{-3}$ and $\Delta\rho$ is the change in water density due to a cooling ΔT and a freshening ΔS , with α and β being the thermal and salin-

ity expansion coefficients, respectively. The relative importance of freshening versus cooling can be quantified by the ratio $R = \beta \Delta S / \alpha \Delta T$. For a freshwater input per unit area ΔH and a surface layer of depth H , the change in temperature is given by $\Delta T = (L_f / c_p) (\Delta H / H)$, where $L_f = 0.33 \text{ J kg}^{-1}$ is the latent heat of fusion of ice and $c_p = 4.2 \times 10^{-3} \text{ J kg}^{-1} \text{ K}^{-1}$ is the specific heat capacity of water. The change in salinity is given by $\Delta S = S (\Delta H / H)$. Inserting these relationships gives $R = (\beta / \alpha) (S c_p / L_f)$. For $T = 0^\circ \text{C}$ and $S = 36$ psu, the linearized expansion coefficients are $\alpha = 0.75 \times 10^{-4} \text{ K}^{-1}$ and $\beta = 7.8 \times 10^{-4} \text{ psu}^{-1}$. This implies that $R \equiv 4.7$, meaning that the stabilization of the water column due to freshening dominates destabilization due to cooling by a factor of 4.7. Based on this, we neglect the cooling effect of iceberg melt.

Based on the calculations above, we perform an additional LGM iceberg simulation. In this simulation, a local sea ice cover is added ($A_i = 1$), which causes the wind-driven wave erosion to be turned off ($M_e = 0$), during the 4 coldest winter months (December–March). This is the only difference between this iceberg simulation and the LGM iceberg simulations described above which have $A_i = 0$ throughout the year. The effect of this idealized representation of a local sea ice cover is dramatic: Fig. 2c and f show LGM iceberg trajectories and meltwater flux for the case where $A_i = 1$ during 4 months of the year. Compared to the earlier rapid eastward decline of freshwater input, we now obtain a much more gradual decline that is in agreement with the IRD distribution in sediment cores.

We also consider the impact of varying the duration of the local sea ice cover, setting $A_i = 1$ during periods ranging from one to 11 months. The difference between the sediment IRD thickness and the simulated iceberg meltwater distribution is indicated in Fig. S2 for each duration of sea-ice cover around the icebergs. We find that the sediment IRD distribution is best matched by LGM simulations when sea ice is present for 4 months of the year (Fig. 3b), with scenarios of longer-lasting or shorter-lasting sea ice covers overestimating and underestimating the east–west gradient, respectively (Figs. 3 and S2).

The results presented in this section support the plausibility of the proposed mechanism. Substantial uncertainties should nonetheless be noted. Wave erosion is the result of complex processes that include calving of overhanging slabs (Savage, 2001) and the breakup of large sections due to hydrostatic stresses (Scambos et al., 2005; Wagner et al., 2014). Such processes likely contribute to making the overall breakup behavior of icebergs resemble that of brittle fragmentation (Tournadre et al., 2016). However, current iceberg models do not explicitly represent these processes.

The distribution of initial iceberg sizes used here is based on modern-day observations around Greenland, and calving sizes were likely different for the Laurentide Ice Sheet. This may lead to different meltwater distributions, with larger icebergs transporting relatively more meltwater east. However, considering the meltwater distributions of the individual iceberg size classes used here, we find that meltwater input decays rapidly with longitude for all iceberg sizes (Fig. S3). Furthermore, Fig. S3 shows that the zonal meltwater distributions of the 5 largest initial iceberg sizes ($L = 600\text{--}1500 \text{ m}$) are broadly similar, suggesting that the initial calving size may not greatly impact this distribution. Current standard iceberg decay models are not well suited for modeling much larger icebergs because breakup is not accounted for. Note that previous studies of icebergs in the LGM (Jongma et al., 2013; Roberts et al., 2014), as well as of modern-day Antarctic icebergs (e.g., Gladstone et al., 2001; Martin and Adcroft, 2010; Stern et al., 2016), typically use iceberg size distributions similar to that of Bigg et al. (1997), with iceberg lengths $L \lesssim 2 \text{ km}$, despite the occurrence of larger tabular icebergs in the real world.

The distribution of IRD within the iceberg has been assumed to be uniform, whereas IRD may be more concentrated in the bottom layers of an iceberg (Dowdeswell and Murray, 1990; Death et al., 2006), which could skew the deposition pattern. However, since ablation occurs primarily on the sides rather than the bottom of icebergs, the vertical distribution of IRD within icebergs may not dramatically influence the relationship between IRD discharge and freshwater discharge.

Other errors could arise from inaccuracies in the GCM simulation of the LGM climate. Efforts are underway to obtain more accurate representations of the LGM climate using state estimates that combine paleoproxy records with a GCM (Dail et al., 2014; Kurahashi-Nakamura et al., 2017).

Finally, the model simulates non-interactive icebergs that are forced by precomputed GCM fields. We therefore do not account for feedbacks between the freshwater released by the icebergs and the upper ocean, nor for iceberg–atmosphere interactions. A more comprehensive approach would be to include the icebergs as a fully interactive component of the GCM (e.g., Martin and Adcroft, 2010).

5. Conclusion

We summarize the main results of this study as follows:

- Under the assumption that sea ice concentration around icebergs is negligible, the LGM and 20th century climates allow broadly similar simulated iceberg trajectories and meltwater distributions. Notably, LGM icebergs travel on average approximately the same distance as 20th century icebergs. This can be explained by compensating effects of slower melt and slower iceberg velocities during the LGM. The range of LGM icebergs extends $\sim 8^\circ$ further east in our simulations, which is associated with their release location being $\sim 8^\circ$ further east than the 20th century icebergs.
- Freshwater input declines too rapidly with longitude in the iceberg model simulations compared with Heinrich event IRD layer thicknesses in ocean sediment cores.
- We propose a mechanism involving local wintertime sea ice around the icebergs that could have led to a larger spatial distribution of iceberg meltwater and IRD. The mechanism invokes large densely packed groups of icebergs creating a strong local halocline, which facilitates wintertime sea ice growth. The sea ice damps the waves that would otherwise have eroded the icebergs, thereby leading to longer iceberg lifetimes and a large range of meltwater and IRD release.
- We show that simulations that include a sea ice cover around the icebergs during part of the winter produce a reduced rate of melting and a more spread-out freshwater distribution that varies less with longitude. Back-of-the-envelope calculations suggest that a local sea ice cover around the icebergs may have persisted for four months of the year. Simulations that have sea ice around the icebergs during four months of the year produce a freshwater distribution that agrees with the sediment core IRD thicknesses.

Acknowledgements

This work was supported by National Science Foundation grants OCE-1357078, OPP-1643445, OPP-1744835, and OCE-1357522 and NASA grants NNX13AP60G and NNX14AH87G.

Appendix A. Supplementary material

Supplementary material related to this article can be found online at <https://doi.org/10.1016/j.epsl.2018.05.006>.

References

- Bigg, G.R., Wadley, M.R., Stevens, D.P., Johnson, J.A., 1997. Modelling the dynamics and thermodynamics of icebergs. *Cold Reg. Sci. Technol.* 26 (2), 113–135.
- Brady, E.C., Otto-Bliesner, B.L., Rosenbloom, N., Kay, J.E., 2013. Sensitivity to glacial forcing in the CCSM4. *J. Climate* 26 (6), 1901–1925.
- Broecker, W.S., 1994. Massive iceberg discharges as triggers for global climate change. *Nature* 372 (6505), 421–424.
- Broecker, W.S., Peteet, D.M., Rind, D., 1985. Does the ocean–atmosphere system have more than one stable mode of operation. *Nature* 315 (6014), 21–26.
- Bügelmayer, M., Roche, D.M., Renssen, H., 2015. How do icebergs affect the Greenland ice sheet under pre-industrial conditions? A model study with a fully coupled ice-sheet-climate model. *Cryosphere* 9 (3), 821–835.
- Dail, H., Wunsch, C., Dail, H., Wunsch, C., 2014. Dynamical reconstruction of upper-ocean conditions in the Last Glacial Maximum Atlantic. *J. Climate* 27 (2), 807–823.
- Death, R., Siegert, M.J., Bigg, G.R., Wadley, M.R., 2006. Modelling iceberg trajectories, sedimentation rates and meltwater input to the ocean from the Eurasian Ice Sheet at the Last Glacial Maximum. *Palaeogeogr. Palaeoclimatol. Palaeoecol.* 236 (1–2), 135–150.
- Dowdeswell, J.A., Maslin, M.A., Andrews, J.T., McCave, I.N., 1995. Iceberg production, debris rafting, and the extent and thickness of Heinrich layers (H-1, H-2) in North Atlantic sediments. *Geology* 23 (4), 301–304.
- Dowdeswell, J.A., Murray, T., 1990. Modelling rates of sedimentation from icebergs. In: *Modelling rates of sedimentation from icebergs*. *Geol. Soc. (Lond.) Spec. Publ.* 53 (1), 121–137.
- Gent, P.R., Danabasoglu, G., Donner, L.J., Holland, M.M., Hunke, E.C., Jayne, S.R., Lawrence, D.M., Neale, R.B., Rasch, P.J., Vertenstein, M., Worley, P.H., Yang, Z.-L., Zhang, M., 2011. The Community Climate System Model Version 4. *J. Climate* 24 (19), 4973–4991.
- Gladstone, R.M., Bigg, G.R., Nicholls, K.W., 2001. Iceberg trajectory modeling and meltwater injection in the Southern Ocean. *J. Geophys. Res.* 106 (C9), 19903–19915.
- Heinrich, H., 1988. Origin and consequences of cyclic ice rafting in the Northeast Atlantic Ocean during the past 130 000 years. *Quat. Res.* 29 (2), 142–152.
- Hemming, S.R., 2004. Heinrich events: massive late Pleistocene detritus layers of the North Atlantic and their global climate imprint. *Rev. Geophys.* 42 (1), RG1005.
- Holloway, G., Dupont, F., Golubeva, E., Häkkinen, S., Hunke, E., Jin, M., Karcher, M., Kauker, F., Maltrud, M., Morales Maqueda, M.A., Maslowski, W., Platov, G., Stark, D., Steele, M., Suzuki, T., Wang, J., Zhang, J., 2007. Water properties and circulation in Arctic Ocean models. *J. Geophys. Res., Atmos.* 112 (C4), 529–545.
- International Ice Patrol, 2009. What is the extreme range of iceberg locations? www.navcen.uscg.gov (Accessed 25 May 2017).
- Jongma, J.I., Driesschaert, E., Fichet, T., Goosse, H., Renssen, H., 2009. The effect of dynamic–thermodynamic icebergs on the Southern Ocean climate in a three-dimensional model. *Ocean Model.* 26 (1–2), 104–113.
- Jongma, J.I., Renssen, H., Roche, D.M., 2013. Simulating Heinrich event 1 with interactive icebergs. *Clim. Dyn.* 40 (5–6), 1373–1385.
- Kurahashi-Nakamura, T., Paul, A., Losch, M., 2017. Dynamical reconstruction of the global ocean state during the Last Glacial Maximum. *Paleoceanography* 32, 326–350.
- Levine, R.C., Bigg, G.R., 2008. Sensitivity of the glacial ocean to Heinrich events from different iceberg sources, as modeled by a coupled atmosphere–iceberg–ocean model. *Paleoceanography* 23 (4), PA4213.
- Manabe, S., Stouffer, R.J., 1997. Coupled ocean–atmosphere model response to freshwater input: comparison to Younger Dryas Event. *Paleoceanography* 12 (2), 321–336.
- Marsh, R., Ivchenko, V.O., Skliris, N., Alderson, S., Bigg, G.R., Madec, G., Blaker, A.T., Aksenov, Y., Sinha, B., Coward, A.C., Le Sommer, J., Merino, N., Zalesny, V.B., 2015. NEMO-ICB (v1.0): interactive icebergs in the NEMO ocean model globally configured at eddy-permitting resolution. *Geosci. Model Dev.* 8 (5), 1547–1562.
- Martin, T., Adcroft, A., 2010. Parameterizing the fresh-water flux from land ice to ocean with interactive icebergs in a coupled climate model. *Ocean Model.* 34 (3–4), 111–124.
- McGee, D., Broecker, W.S., Winckler, G., 2010. Gustiness: the driver of glacial dustiness? *Quat. Sci. Rev.* 29 (17–18), 2340–2350.
- Otto-Bliesner, B.L., Brady, E.C., 2010. The sensitivity of the climate response to the magnitude and location of freshwater forcing: last glacial maximum experiments. *Quat. Sci. Rev.* 29 (1–2), 56–73.
- Rhodes, R.H., Brook, E.J., Chiang, J.C.H., Blunier, T., Maselli, O.J., McConnell, J.R., Romanini, D., Severinghaus, J.P., 2015. Enhanced tropical methane production in response to iceberg discharge in the North Atlantic. *Science* 348 (6238), 1016–1019.
- Roberts, W.H.G., Valdes, P.J., Payne, A.J., 2014. A new constraint on the size of Heinrich Events from an iceberg/sediment model. *Earth Planet. Sci. Lett.* 386, 1–9.
- Savage, S.B., 2001. Aspects of iceberg deterioration and drift. In: *Geomorphological Fluid Mechanics*. Springer, Berlin, Heidelberg, pp. 279–318.
- Scambos, T., Sergienko, O., Sargent, A., MacAyeal, D., Fastook, J., 2005. ICESat profiles of tabular iceberg margins and iceberg breakup at low latitudes. *Geophys. Res. Lett.* 32 (23).
- Stern, A.A., Adcroft, A., Sergienko, O., 2016. The effects of Antarctic iceberg calving-size distribution in a global climate model. *J. Geophys. Res., Oceans* 121, JC011835.
- Sulak, D.J., Sutherland, D.A., Enderlin, E.M., Stearns, L.A., Hamilton, G.S., 2017. Iceberg properties and distributions in three Greenlandic fjords using satellite imagery. *Ann. Glaciol.* 58 (74), 92–106.
- Tournadre, J., Bouhier, N., Girard-Ardhuin, F., Remy, F., 2016. Antarctic icebergs distributions 1992–2014. *J. Geophys. Res., Oceans* 121 (1), 327–349.
- Wagner, T.J.W., Dell, R.W., Eisenman, I., 2017a. An analytical model of iceberg drift. *J. Phys. Oceanogr.* 47 (7), 1605–1616.
- Wagner, T.J.W., Eisenman, I., 2015. False alarms: how early warning signals falsely predict abrupt sea ice loss. *Geophys. Res. Lett.* 42 (23), 10,333–10,341.
- Wagner, T.J.W., Eisenman, I., 2017. How climate model biases skew the distribution of iceberg meltwater. *Geophys. Res. Lett.* 26 (2), 113.
- Wagner, T.J.W., Stern, A.A., Dell, R.W., Eisenman, I., 2017b. On the representation of capsizing in iceberg models. *Ocean Model.* 117, 88–96.
- Wagner, T.J.W., Wadhams, P., Bates, R., Elosegui, P., Stern, A., Vella, D., Abrahamsen, P., Crawford, A., Nicholls, K.W., 2014. The “footloose” mechanism: iceberg decay from hydrostatic stresses. *Geophys. Res. Lett.* 41, 5522–5529.